X-ray response to disk evolution in two γ Cas stars

Yaël Nazé, Gregor Rauw, Terrence Bohlsen, Bernard Heathcote, Padric Mc Gee, Paulo Cacella, Christian Motch

Monthly Notices of the ROYAL ASTRONOMICAL SOCIETY

MNRAS **512,** 1648–1657 (2022) https://doi.org/10.1093/mnras/stac314
Advance Access publication 2022 February 7

X-ray response to disc evolution in two γ Cas stars

Yaël Nazé [1]★† Gregor Rauw [1] Terrence Bohlsen [2] Bernard Heathcote,[3] Padric Mc Gee,[4] Paulo Cacella[5] and Christian Motch[6]

[1]*Groupe d'Astrophysique des Hautes Energies, STAR, Université de Liège, Quartier Agora (B5c, Institut d'Astrophysique et de Géophysique), Allée du 6 Août 19c, B-4000 Sart Tilman, Liège, Belgium*
[2]*SASER/Mirranook Observatory, Armidale, NSW 2350, Australia*
[3]*SASER, 269 Domain Road, South Yarra, VIC 3141, Australia*
[4]*SASER/Department of Physics, University of Adelaide, Adelaide, SA 5005, Australia*
[5]*DogsHeaven Observatory, SMPW Q25 CJ1 LT10, Brasilia 71745-501, DF, Brazil*
[6]*Observatoire Astronomique de Strasbourg, Université de Strasbourg, CNRS, UMR 7550, F-67000 Strasbourg, France*

Accepted 2022 January 27. Received 2022 January 24; in original form 2021 December 3

ABSTRACT

The Hα emission of a set of southern γ Cas stars was monitored since 2019, with the aim of detecting transition events and examining how their peculiar X-ray emission would react in such cases. Two stars, namely HD 119682 and V767 Cen, were found to display slowly decreasing disc emissions. These decreases were not perfectly monotonic and several temporary and limited rebuilding events were observed. For HD 119682, the emission component in Hα disappeared in 2020 mid-July. In X-rays, the X-ray flux was twice smaller than that recorded two decades ago but of a similar level as observed a decade ago. The X-ray flux decreased over the campaign by 30 per cent, but the hardness remained similar in data sets of all epochs. In particular, the γ Cas character remained as clear as before even when there was no trace of disc emission in the Hα line. For V767 Cen, the full disappearance of disc emission in Hα never occurred. We followed closely a disc rebuilding event, but no significant change in flux or hardness was detected. These behaviours are compared to those of other γ Cas stars and their consequences on the X-ray generation are discussed.

Key words: stars: early-type – stars: emission-line, Be – stars: massive – stars: variables: general – X-rays: stars.

1 INTRODUCTION

The vast majority of stars are known X-ray emitters, and the most massive ones are no exception. The cause of their high-energy emission lies in the material ejected by those stars. The stellar winds of OB stars are driven by the scattering of the ultraviolet (UV) radiation by metallic ions. This driving process is intrinsically unstable and the resulting shocks lead to the generation of X-rays (Feldmeier, Puls & Pauldrach 1997). This wind emission is soft (plasma temperature of about 0.6 keV) and rather faint [log (L_X/L_{BOL}) ~ -7]. If a large-scale magnetic field is present, the wind flows can be channelled by the field and collide, generating hot plasma. This leads to an additional X-ray emission, generally harder in character (ud-Doula & Nazé 2016). Alternatively, when two massive stars form a binary system, the two winds may collide and the strong shock may generate X-rays (Rauw & Nazé 2016): some massive binary systems thus appear harder (plasma temperature of about 2.0 keV) and brighter [log (L_X/L_{BOL}) up to -6]. Finally, a small subgroup of stars have emerged in the last decade: the γ Cas analogues (Smith, Lopes de Oliveira & Motch 2016). These stars also display thermal X-ray spectra, but much harder (plasma temperature >5 keV) and brighter [log (L_X/L_{BOL}) between -6.2 and -4]. Only X-ray binaries (XRBs) appear brighter in the X-ray range than those γ Cas stars. It must be noted that all of these objects are of the Oe/Be spectral type; i.e. they possess a decretion disc. However, up to now, the only difference spotted between the other Oe/Be stars and the γ Cas analogues resides in their X-ray properties (Nazé, Rauw & Pigulski 2020; Nazé et al. 2021).

While the link between the outflows and the X-ray emission is well understood for the other cases (embedded wind shocks, magnetically confined winds, and colliding winds), the origin of the peculiar γ Cas characteristics remains debated. Up to now, all detected γ Cas analogues belong to the Oe/Be category; i.e. they possess a decretion disc in Keplerian rotation. This gives us an important clue, but the exact role of the disc in the generation of the high-energy emission remains unclear. In this context, two broad classes of scenarios to explain the γ Cas phenomenon have been proposed. The first one relies on the presence of a companion. It could be a compact object (white dwarf or neutron star) and the X-rays would then come from its accretion of material from the Be star and its disc (Murakami et al. 1986; Postnov, Oskinova & Torrejón 2017). In such a case, if the disc dissipates, the source of material disappears; hence, the X-ray emission should ultimately (i.e. after some travelling delay) stop. Another possibility is to consider a stripped He-star companion whose stellar wind collides with the peripheral regions of the disc, thereby leading to a possible emission of X-rays (Langer et al. 2020). Again, the disappearance of the disc implies cutting the feeding of the X-ray source. In contrast, the second type of scenario requires no

★ E-mail: ynaze@uliege.be
† F.R.S.-FNRS Senior Research Associate.

companion as it involves magnetic interactions between the Be star and its inner disc (Robinson, Smith & Henry 2002; Motch, Lopes de Oliveira & Smith 2015). In such a case, if the disc fully dissipates, the interactions will no longer take place; hence, the peculiar X-ray emission should disappear, with a faster reaction time than for the previous case. Similar arguments can be built perforce if considering a disc outburst rather than a disc dissipation. Following the behaviour of the X-ray emission in reaction to changes in the disc therefore has an important diagnostic value. In this context, long-term monitorings are required as they are the only way to assess the amplitude of the correlated X-ray response to an optical event (if any) and to derive the time lag between them (if any).

In this paper, we present the results of such an exercise for two γ Cas stars, namely HD 119682 and V767 Cen. The γ Cas nature of HD 119682 (B0Ve, $V = 7.9$) was first reported by Rakowski et al. (2006) and Safi-Harb et al. (2007). Indeed, the X-ray emission is both much harder (plasma temperature of ∼10 keV, hard-to-soft flux ratio of 2.5) and brighter [$\log(L_X/L_{BOL}) \sim -5.7$] than that of ordinary OB stars (Nazé & Motch 2018). The star was also classified as a binary candidate in Nazé et al. (2021). The X-ray emission of V767 Cen (HD 120991, B2Ve, $V = 6.1$) was studied in detail by Nazé & Motch (2018) thanks to an *XMM–Newton* archival exposure. The star displayed a $\log(L_X/L_{BOL}) \sim -5.4$, a plasma temperature of 6.4 keV, and a hard-to-soft flux ratio of 2, all pointing to a γ Cas nature. Unfortunately, no optical data were available for the two stars at the time of these discovery observations. However, our optical monitoring fills this gap and enlarges the view by revealing changes in their discs. X-ray observations were then triggered to assess the reaction of the high-energy emission to the disc variations. Section 2 presents the data used in this study, while Section 3 derives the results, Section 4 discusses them, and Section 5 summarizes them.

2 DATA

2.1 Optical data

To ensure a regular monitoring of the Hα line, we set up a collaboration with amateur astronomers. Since 2019, four persons regularly observed a set of southern Be stars, with three observers (co-authors TB, BH, and PMcG) based in Australia and one (co-author PC) in Brazil. Their instruments were 11–14-inch reflectors equipped with spectrographs (Gerlach LowSpec, Shelyak LHIRESIII, LISA, eShel) that provided spectral resolutions between 400 and 20 000 (most common value was ∼4000 for HD 119682 and ∼10 000 for the brighter V767 Cen). For HD 119682, exposure times ranged from 5 min to 3.5 h, leading to typical signal-to-noise ratios of 75; for V767 Cen, exposure times were similar but average signal-to-noise ratio was 50. The spectra were reduced in a standard way using ISIS[1] and finally normalized over the same set of continuum windows using polynomials of low order. No telluric correction could be made for the low-resolution spectra (all HD 119682 data and a quarter of V767 Cen data), but it was applied for observations taken with higher resolution. All Australian amateur spectra were deposited on the Be Star Spectra (BeSS) open-access data base (Neiner et al. 2011)[2]. Note that HD 119682 belongs to a small group made of several stars, notably CPD–62°3559 (K 2 II/III) and HD 119699 (A 1 II), but their spectral types being different from that of HD 119682 and their separation being large enough, the amateur spectra of HD 119682 were not contaminated by these close neighbours.

In parallel, a few spectra of both stars were obtained at the Cerro Paranal ESO (European Southern Observatory) Observatory for our ESO programme ID 105.204D. They were taken with the Ultraviolet and Visual Echelle Spectrograph (UVES) in dichroic mode (covered regions: 3300–4560 Å at $R \sim 70\,000$ and 4730–6830 Å at $R \sim 100\,000$). These spectra were already used and presented in Nazé et al. (2021), and we refer to that publication for details on this data set. An additional X-Shooter spectrum of each star was also taken for the same programme. Their spectral resolution is lower than that of UVES ($R \sim 20\,000$ in the visible range) but the signal-to-noise ratios are high (∼200). These spectra were reduced in the same way as the UVES data.

Hα equivalent widths (EWs) were estimated for all spectra using the first-order moment over a given velocity range (−600 to 600 km s^{-1}). They are listed in Tables 1 and 2 for HD 119682 and V767 Cen, respectively.

Contemporaneous photometry was recorded by the All-Sky Automated Survey for SuperNovae (ASAS-SN)[3] for both stars. The targets are, however, brighter than the saturation limit of ASAS-SN. In such cases, a correction procedure using the bleed trails is

Table 1. EWs measured on Hα (in the −600 to +600 km s^{-1} interval) for HD 119682.

Date	ID	EW (Å)	Date	ID	EW (Å)
8564.993	BH^n	− 4.29 ± 0.12	9049.936	TB	1.25 ± 0.02
8573.977	TB	− 3.81 ± 0.03	9053.961	PMcG^l	1.12 ± 0.02
8580.956	TB	− 3.53 ± 0.03	9057.953	PMcG^l	1.22 ± 0.03
8602.994	BH^n	− 3.04 ± 0.05	9060.885	BH^l	1.12 ± 0.04
8610.011	BH^n	− 3.12 ± 0.11	9061.954	TB	1.21 ± 0.03
8661.063	PMcG^l	0.07 ± 0.07:	9074.952	TB^l	0.80 ± 0.03
8662.012	TB^l	− 1.03 ± 0.06	9080.974	TB	0.59 ± 0.04
8676.913	TB	− 0.19 ± 0.02	9089.902	BH^l	0.00 ± 0.07
8682.954	TB	0.14 ± 0.02	9098.880	BH^l	0.34 ± 0.07
8698.991	TB	0.30 ± 0.03	9185.837	UVES	1.650 ± 0.003
8713.963	TB	1.06 ± 0.03	9205.842	UVES	1.639 ± 0.003
8719.949	TB	1.15 ± 0.02	9218.850	Xsh	1.007 ± 0.012
8721.940	TB	0.97 ± 0.02	9234.113	PMcG^l	1.39 ± 0.04
8724.925	PMcG	0.21 ± 0.06	9242.753	UVES	1.186 ± 0.003
8728.935	TB	0.99 ± 0.03	9256.984	TB	1.25 ± 0.05
8756.956	PMcG^n	1.42 ± 0.27	9257.801	UVES	1.226 ± 0.004
8837.225	PMcG^n	− 3.06 ± 0.14	9274.662	UVES	− 0.294 ± 0.003
8865.210	PMcG^n	− 2.68 ± 0.13	9275.999	TB	− 0.53 ± 0.03
8878.205	PMcG	− 1.98 ± 0.06	9277.079	PMcG^l	− 0.27 ± 0.04
8934.002	PMcG^n	1.92 ± 0.17	9297.953	TB	− 0.88 ± 0.03
8952.069	TB	1.06 ± 0.03	9329.994	TB	− 0.74 ± 0.02
8974.035	PMcG^l	1.36 ± 0.07	9331.188	PMcG^l	− 0.60 ± 0.05
8981.055	TB	1.75 ± 0.02	9364.989	BH^l	0.98 ± 0.03
9017.003	TB	1.57 ± 0.02	9371.045	TB	1.07 ± 0.02
9037.950	TB	1.51 ± 0.03	9394.925	PMcG^l	1.07 ± 0.03
9044.996	TB	1.48 ± 0.03	9424.977	TB	0.77 ± 0.03
9045.021	PMcG^l	1.36 ± 0.04	–	–	–

Notes. Dates are in the format HJD-2 450 000, and ':' indicates an uncertain value. The ID refers to the source of the spectrum: UVES or Xsh for the ESO data, TB, BH, PMcG, or PC for the amateur data (from their initials; see authors' list). Symbols ^{n} and ^{l} are added for the noisier spectra (SNR < 20) and lower resolution data ($R < 3000$ but SNR > 20), respectively. Note that the errors on EWs are computed from flux errors. They only reflect the SNR and do not include the normalization errors.

[1] http://www.astrosurf.com/buil/isis-software.html
[2] http://basebe.obspm.fr
[3] https://asas-sn.osu.edu/

Table 2. Same as in Table 1 for V767 Cen, except that low resolution is here defined as $R < 5000$.

Date	ID	EW (Å)	Date	ID	EW (Å)
8570.959	TB	− 8.25 ± 0.01	9116.885	TB	− 3.55 ± 0.01
8578.070	BH	− 7.46 ± 0.03	9127.873	TB	− 2.15 ± 0.03
8590.038	BH	− 7.09 ± 0.02	9191.842	UVES	− 3.981 ± 0.002
8599.002	TB	− 7.15 ± 0.01	9196.843	Xsh	− 3.889 ± 0.013
8610.154	PMcG^{l}	− 8.94 ± 0.03	9206.834	UVES	− 3.436 ± 0.003
8624.000	BH	− 10.29 ± 0.02	9231.859	UVES	− 2.502 ± 0.003
8641.155	PMcG^{l}	− 7.68 ± 0.05	9234.149	PMcG^{l}	− 2.64 ± 0.03
8655.954	PMcG^{l}	− 8.07 ± 0.08	9246.777	UVES	− 1.864 ± 0.002
8668.932	BH	− 7.88 ± 0.02	9298.965	TB	− 2.24 ± 0.01
8683.984	PMcG^{l}	− 7.39 ± 0.02	9335.978	TB	− 3.42 ± 0.01
8684.995	TB	− 7.30 ± 0.01	9351.943	TB	− 2.31 ± 0.01
8685.943	BH	− 7.31 ± 0.03	9364.964	BH^{l}	− 0.96 ± 0.03
8693.970	TB	− 7.31 ± 0.01	9368.914	BH	− 0.91 ± 0.04
8697.971	TB	− 7.76 ± 0.02	9370.923	TB	− 1.62 ± 0.01
8724.949	PMcG^{l}	− 6.85 ± 0.03	9381.914	BH	− 0.62 ± 0.03
8728.953	TB^{l}	− 5.99 ± 0.03	9386.933	BH	− 1.05 ± 0.03
8865.177	PMcG^{l}	− 5.01 ± 0.05	9394.989	PMcG^{l}	− 0.33 ± 0.04
8934.037	PMcG^{l}	− 2.15 ± 0.04	9398.501	PC	− 0.13 ± 0.04
8937.978	TB	− 2.42 ± 0.02	9399.534	PC	− 0.36 ± 0.03
8948.992	BH	− 2.56 ± 0.05	9401.876	PMcG^{l}	− 0.91 ± 0.03
8953.044	PMcG^{l}	− 2.85 ± 0.03	9403.964	BH	− 0.78 ± 0.03
8960.996	BH	− 3.41 ± 0.02	9406.467	PC	− 1.33 ± 0.02
8962.024	TB	− 3.42 ± 0.01	9406.977	TB	− 2.00 ± 0.01
8972.955	TB	− 3.10 ± 0.02	9407.505	PC	− 1.50 ± 0.03
8974.080	PMcG^{l}	− 3.34 ± 0.03	9408.465	PC	− 2.17 ± 0.02
8975.994	TB	− 2.92 ± 0.02	9410.462	PC	− 1.92 ± 0.03
8984.037	BH	− 3.68 ± 0.03	9421.462	PC	− 4.08 ± 0.03
8995.951	BH	− 2.92 ± 0.03	9422.959	TB	− 4.62 ± 0.01
8998.034	TB	− 2.70 ± 0.02	9424.973	BH^{l}	− 4.05 ± 0.02
9003.996	TB	− 2.46 ± 0.02	9426.474	PC	− 3.76 ± 0.03
9015.943	TB	− 1.61 ± 0.02	9428.909	BH^{l}	− 3.66 ± 0.01
9018.024	BH	− 1.35 ± 0.04	9429.473	PC	− 4.06 ± 0.03
9029.970	BH	− 2.11 ± 0.03	9435.442	PC	− 4.39 ± 0.03
9031.971	TB	− 2.19 ± 0.02	9437.976	TB	− 4.55 ± 0.01
9044.996	BH	− 3.28 ± 0.02	9441.447	PC	− 4.07 ± 0.02
9045.074	PMcG^{l}	− 3.26 ± 0.02	9445.908	BH	− 3.42 ± 0.03
9062.973	BH	− 3.33 ± 0.04	9446.994	TB	− 3.81 ± 0.02
9066.997	TB	− 3.09 ± 0.02	9456.907	BH	− 2.99 ± 0.04
9071.891	BH^{l}	− 2.46 ± 0.03	9459.969	TB	− 3.49 ± 0.02
9074.983	TB	− 2.80 ± 0.02	9466.915	TB	− 2.99 ± 0.02
9106.910	BH^{n}	− 1.56 ± 0.06	9481.916	TB	− 1.97 ± 0.02
9111.496	UVES	− 2.312 ± 0.002	9591.165	PMcG	− 1.50 ± 0.02
9112.914	BH^{n}	− 3.32 ± 0.07	–	–	–

implemented, but it is far from perfect and notably requires the targets to be isolated (ASAS-SN has a point spread function of 15 arcsec full width at half-maximum). For HD 119682, which lies in a crowded area, the data points are unrealistically spread over several magnitudes and the light curve is unusable. For V767 Cen, the situation appears better, although a dispersion of ∼0.07 mag is present (which cannot hide long-term trends if present; see e.g. a similar situation for π Aqr in Nazé, Rauw & Smith 2019). Only g-band data cover the dates of our monitoring. A few outliers (having values deviating from the median by 3 times the median absolute deviations) were filtered out.

2.2 X-ray observations

Both of our targets were observed with *XMM–Newton*. The first observation of HD 119682 was taken in 2001 August in full frame mode and with a thick filter to avoid contamination by UV/optical photons (40 ks, Rev. 315, ObsID = 0087940201, PI: Hughes). HD 119682 here appears off-axis as the observation was concerned with a nearby supernova remnant. The star was re-observed on-axis in 2009 March (54 ks, Rev. 1692, ObsID = 0551000201, PI: Motch), this time with a medium filter. Finally, we triggered our target-of-opportunity (TOO) programme to monitor the X-ray emission of HD 119682 as its disc was disappearing, leading to four additional observations taken with the medium filter and in large window mode (PI: Rauw; 10 ks in 2019 August on Rev. 3610, ObsID = 0840310901; 20 ks in 2020 January on Rev. 3684, OBsID = 0840311001; 10 ks in 2020 July for Rev. 3775, ObsID = 0840311101 and 2021 March for Rev. 3890, ObsID = 0840310801).

XMM–Newton also observed V767 Cen during 7 ks in 2007 January (Rev. 1306, ObsID = 0402121801, PI: Favata) using a thick filter and the large window mode. Following the observation of a disc flaring (see below), we requested a TOO observation that was taken in 2021 July with the same characteristics as in the first pointing (Rev. 3967, ObsID = 0891800801, PI: Nazé).

All *XMM–Newton* data were processed with the Science Analysis Software (SAS) v19.1.0 using calibration files available in 2021 June and following the recommendations of the *XMM–Newton* team.[4] The European Photon Imaging Camera (EPIC) observations were first processed with the pipeline and then filtered to keep only the best-quality data (PATTERN 0–12 for MOS and 0–4 for pn). To assess whether contamination by background proton flares was present, we built global light curves for energies above 10 keV and discarded time intervals corresponding to flares. Only the older two data sets and that of 2020 July were affected by such flares for HD 119682, while there was no flare for the V767 Cen data. Source detection was then performed to assess the crowding in the fields of view. This allowed us to carefully choose extraction regions. The source regions were circles centred on the Simbad positions of the targets and with radii of 30 arcsec in general, while background regions were chosen from nearby circles devoid of sources and generally 50 arcsec in radius. Background-corrected light curves were calculated for energy bands of 0.5–10.0, 0.5–2.0, and 2.0–10.0 keV. For HD 119682, bins of 100 s and 1 ks were used, whereas shorter bins of 50 and 500 s could be used for V767 Cen to get the same light-curve quality since its X-ray flux is larger. The light curves were corrected for vignetting, off-axis angle, and bad pixels, and bins exposed during less than half nominal bin length were eliminated. For spectra, dedicated calibration matrices were built and a grouping was then applied to obtain an oversampling factor of maximum 5 and a minimum signal-to-noise ratio of 3.

For HD 119682, a few *Chandra* observations were also available. These grating observations were taken in 2008 December (ObsID = 8929 and 10834–6, PI: Rakowski), totalling nearly 150 ks altogether. Individual zeroth-order spectra as well as combined (order +1 and −1) grating spectra were extracted for high- and medium-energy gratings (HEG and MEG, respectively). The reduction of these observations was presented in Nazé & Motch (2018) and no further processing was applied for this paper. As mentioned in Nazé & Motch (2018), additional *Chandra* observations of HD 119682 were taken with the Advanced CCD Imaging Spectrometer optimized for imaging (ACIS-I) and suffer from pile-up; hence, they could not be used.

For V767 Cen, we further obtained an X-ray monitoring with the Neil Gehrels *Swift* observatory (ObsID = 00014422001–8) during the second semester of 2021 and early 2022. The X-ray

[4]For SAS threads, see http://xmm.esac.esa.int/sas/current/documentation/threads/.

Table 3. Best-fitting models to the X-ray spectra.

ID	I	HJD −2450000	$N_{\rm H}^{ISM}$	$N_{\rm H}$ (10^{22} cm^{-2})	kT (keV)	Norm (10^{-4} cm^{-5})	χ^2/dof	$F_{\rm X}^{\rm obs}$ (tot, 10^{-12} erg cm^{-2} s^{-1})	$F_{\rm X}^{\rm ISM-cor}$	HR
HD 119682										
0315	x	2149.849	0.2	0.020 ± 0.008	7.8 ± 0.4	11.8 ± 0.13	518.71/468	1.90 ± 0.02	2.09	2.24 ± 0.05
8929	c	4817.692	0.2	0.00 ± 0.02	10.3 ± 2.2	11.3 ± 0.39	49.52/56	1.90 ± 0.12	2.10	2.44 ± 0.27
10835	c	4820.076	0.2	0.00 (fixed)	9.4 ± 1.9	8.45 ± 0.33	49.68/45	1.41 ± 0.08	1.55	2.35 ± 0.22
10834	c	4821.515	0.2	0.00 ± 0.03	12.5 ± 2.7	8.58 ± 0.24	106.86/89	1.47 ± 0.07	1.60	2.61 ± 0.19
10836	c	4822.342	0.2	0.06 ± 0.07	12.9 ± 6.0	10.2 ± 0.60	39.87/51	1.70 ± 0.12	1.84	2.91 ± 0.33
comb.	c	4820.201	0.2	0.13 ± 0.13	12.5 ± 8.2	12.0 ± 0.66	128.98/444	1.97 ± 0.12	2.12	3.21 ± 0.38
1692	x	4897.283	0.2	0.009 ± 0.008	8.1 ± 0.5	6.97 ± 0.09	467.69/448	1.13 ± 0.02	1.25	2.24 ± 0.05
3610	x	8721.890	0.2	0.000 ± 0.007	8.3 ± 0.8	6.74 ± 0.11	283.72/268	1.10 ± 0.03	1.22	2.23 ± 0.10
3684	x	8870.137	0.2	0.000 ± 0.005	8.3 ± 0.5	6.94 ± 0.09	396.86/363	1.13 ± 0.02	1.26	2.22 ± 0.07
3775	x	9050.958	0.2	0.00 (fixed)	7.8 ± 0.7	5.86 ± 0.10	270.94/265	0.95 ± 0.03	1.05	2.17 ± 0.09
3890	x	9279.849	0.2	0.000 ± 0.008	8.8 ± 1.1	4.88 ± 0.10	265.48/234	0.81 ± 0.03	0.89	2.29 ± 0.11
V767 Cen										
1306	x	4126.327	0.043	0.065 ± 0.013	0.27 ± 0.03	1.26 ± 0.37	494.27/443	3.09 ± 0.05	3.18	1.97 ± 0.06
	–	–	–	6.48 ± 0.33	18.5 ± 0.28	–	–	–	–	–
3967	x	9434.160	0.043	0.080 ± 0.012	0.28 ± 0.03	1.60 ± 0.39	560.49/451	3.28 ± 0.05	3.38	1.89 ± 0.06
	–	–	–	6.02 ± 0.37	20.0 ± 0.30	–	–	–	–	–
00014422001	s	9409.837	0.043	0.21 ± 0.09	0.28 and 6.02 (fixed)	25.3 ± 2.5	56.46/51	3.85 ± 0.32	3.93	2.37 ± 0.32
00014422002	s	9428.756	0.043	0.10 ± 0.10	0.28 and 6.02 (fixed)	24.5 ± 3.3	30.19/34	3.97 ± 0.41	4.08	1.96 ± 0.35
00014422003+4	s	9446.647	0.043	0.00 ± 0.10	0.28 and 6.02 (fixed)	16.6 ± 2.4	37.16/36	2.88 ± 0.43	2.98	1.61 ± 0.39
00014422005	s	9465.858	0.043	0.09 ± 0.10	0.28 and 6.02 (fixed)	23.7 ± 3.0	36.50/38	3.88 ± 0.36	3.99	1.91 ± 0.31
00014422006	s	9486.837	0.043	0.00 ± 0.08	0.28 and 6.02 (fixed)	20.9 ± 2.6	50.01/48	3.62 ± 0.40	3.76	1.62 ± 0.34
00014422007	s	9561.986	0.043	0.00 ± 0.11	0.28 and 6.02 (fixed)	14.9 ± 2.4	51.76/39	2.59 ± 0.36	2.68	1.63 ± 0.33
00014422008	s	9583.002	0.043	0.00 ± 0.07	0.28 and 6.02 (fixed)	16.6 ± 2.1	35.38/32	2.88 ± 0.38	2.99	1.62 ± 0.35
π Aqr										
00010659001-39	s	8344.345	0.036	0.53 ± 0.06	27.6 ± 9.4	105.5 ± 4.6	396.03/436	16.0 ± 0.4	16.1	6.10 ± 0.24

Notes. Fitted models were of the form tbabs × phabs × apec, with the first absorption fixed to the interstellar value. ID refers to the revolution number (for *XMM–Newton*) or ObsID (for *Chandra*); 'comb' indicates the fitting of the fully combined (all obs, both orders) *Chandra* HEG and MEG grating spectra. Column I identifies the facility used (x for *XMM-Newton*, c for *Chandra*, and s for *Swift*). The hardness ratios are defined by HR = $F_{\rm X}^{\rm ISM-cor}$(hard)/$F_{\rm X}^{\rm ISM-cor}$(soft), with $F_{\rm X}^{\rm ISM-cor}$ the flux after correction for interstellar absorption and soft and hard energy bands being defined as 0.5–2.0 and 2.0–10.0 keV, respectively (the total band being 0.5–10.0 keV). Errors correspond to 1σ uncertainties; they correspond to the larger value if the error bar is asymmetric. For *Swift* spectra of V767 Cen, the normalization factor of the 0.28 keV component is fixed to 0.08 times that of the 6.02 keV component, as in the *XMM–Newton* data of Rev. 3967, and only the normalization of that hottest component is provided here.

telescope was used in windowed timing mode because V767 Cen, with its $V = 6.1$, is too bright in the optical and UV ranges for the other observation mode. Since we were mostly interested in flux variations, exposures were of 2–3 ks duration, allowing for a few hundred counts to be collected for the source. Note that exposures 00014422003–4, taken 4 d apart, were combined to reach the required signal-to-noise. Individual count rates and spectra were obtained with the *Swift* online tool.[5] Note that V767 Cen is at the limit for WT observations: The background has a similar count rate as the source and the centroiding is difficult. Some slight systematic errors cannot be totally excluded, but the consistency of the obtained data advocates for a limited impact on our results.

Spectra were then fitted in XSPEC v12.11.1 using absorbed optically thin thermal emission models with solar abundances from Asplund et al. (2009). For *XMM–Newton*, all EPIC spectra (pn, MOS1, and MOS2) were fitted simultaneously; for *Chandra*, zeroth-order spectra were fitted for individual exposures, while a fit to the HEG and MEG grating spectra combining both orders and all exposures was also made. The chosen models were as in Nazé & Motch (2018). Results are provided in Table 3 – slight differences with those reported in Nazé & Motch (2018) for the same exposures come from the improved atomic parameters of the fitting tool. For V767 Cen, a single temperature fit could a priori provide sufficient results for *Swift* spectra. Nevertheless, two-temperature fits were also tried to ease the comparison with *XMM–Newton* results. As the *Swift* data have lower quality, especially at low energies, the temperatures were fixed to those found with *XMM–Newton*, which show little changes between the two observations. However, even with fixed temperatures, the strength of the low-temperature component could not be constrained. We therefore further fixed the ratio between the normalization factors of the two thermal components to the value observed with *XMM–Newton* in 2021.

[5] https://www.swift.ac.uk/user_objects/

3 RESULTS

3.1 HD 119682

When the optical monitoring began in 2019, the Hα line of HD 119682 displayed a double-peaked emission, with no trace of absorption. The EW was moderate (−4.3 Å, a slightly lower value than in an older – 2017 May – spectrum). Over the course of the year, the emission steadily decreased, with the underlying absorption more and more clearly detectable. A moderate emission suddenly reappeared in 2020 January (EW $\sim$ −3 Å), but disappeared soon afterwards. The Hα line then remained in absorption, although a small emission did shortly reappear in 2020 December and 2021 March–April (Fig. 1). Thus, during the monitoring, the disc did not undergo a monotonic disappearance. Rather, the behaviour appears somewhat erratic, with an overall disappearance trend superimposed on temporary disc reinforcements, probably corresponding to small mass ejection events. The complex emission-line profile, with changing width and even multiple peaks as revealed by ESO spectra, also points towards a complicated disc geometry at those times: The

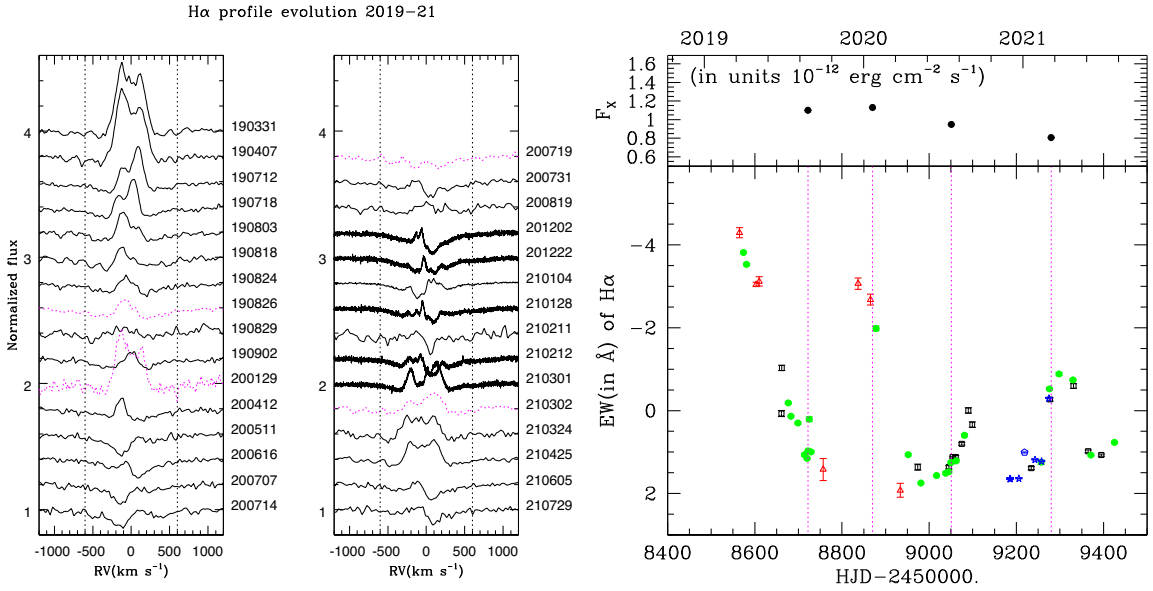

Figure 1. Left-hand panels: Evolution with time of the profile of the Hα line observed in HD 119682 during our monitoring campaign. Dates in YYMMDD are provided to the right of the line. Spectra taken close to the time of an *XMM–Newton* observation are shown with a magenta dotted line, while vertical black dotted lines indicate the interval chosen for EW determination. Note that the noisier (SNR $<$ 20) or lower resolution (R $<$ 3000) spectra are not shown. Right-hand panel: Evolution with time of the Hα EWs measured in the -600 to $+600$ km s^{-1} interval and of X-ray fluxes. The top axis provides the date in years, while the bottom axis uses Julian dates. Red open triangles display the values obtained from the noisier spectra (SNR $<$ 20), black open squares those measured on the lower resolution data (R $<$ 3000 but SNR $>$ 20), green dots those derived from other amateur spectra (R $>$ 3000 and SNR $>$ 20), and blue symbols those measured on ESO spectra (stars for UVES and open pentagon for X-Shooter). Note the very good agreement between ESO and amateur data taken at similar dates. The vertical magenta dotted lines indicate the times of the *XMM–Newton* observations.

ejected material does not seem to form a single blob slowly and smoothly mixing with the disc.

The Hα line profile was very different when the various *XMM–Newton* observations were taken (see magenta profiles in Fig. 1). In 2019 August, the absorption was dominant and the emission weak. In 2020 January, the emission was moderate, while in 2020 July, there was no trace of emission. Finally, in 2021 March, the emission was intermediate between the first two cases. There is unfortunately no information on the shape of the Hα line profile at the time of the older *XMM–Newton* or *Chandra* observations.

During each X-ray observation, short-term flux variations can be spotted in the light curves, as are common in γ Cas stars (e.g. Smith, Lopes de Oliveira & Motch 2012). It should, however, be noted that the count rate does not allow to make light curves with extremely short time bins (e.g. 1 s) thought to be typical of the 'shot'/flaring emission of γ Cas stars; hence, such time-scales remain unexplored for HD 119682. The appendix shows these *XMM–Newton* light curves (Fig. A1). It reveals that the hardness of the emission, estimated from the ratio of hard (2–10 keV) to soft (0.5–2 keV) count rates, does not seem to change in a significant way over the whole *XMM–Newton* data set. With a Pearson correlation coefficient of only 0.33, the hardness also does not appear significantly correlated to the strength of the X-ray emission, estimated from the full band (0.5–10 keV) count rate. Finally, it may be noted that the dispersion of the light-curve points remains similar if one considers a single exposure or the whole data set, despite different values of the average count rate.

Table 3 provides the results of spectral fits. We can see that there is some systematic difference between *XMM–Newton* and *Chandra* results. This is in part due to not only the stellar variations, but also to remaining cross-calibration problems: Even for a stable object, it is quite common to not get exactly the same modelling results. Note that the comparison between the combined grating data and the individual zeroth-order spectra shows a good agreement, indicating little effects of pile-up that could potentially still affect the latter data.

The X-ray flux was about 2×10^{-12} erg cm^{-2} s^{-1} at the time of the oldest observations, but it then decreased by a factor of 2 in more recent years. Focusing on our four monitoring observations, the star did not appear at its lowest flux when the Hα emission was the lowest (absorption only, 2020 July), nor did it appear brighter in 2020 January or 2021 March when a small surge in disc emission occurred. Rather, there seems to be a slow, monotonic flux decline ($\sim$30 per cent) over the entire monitoring interval. Furthermore, restricting to comparing *XMM–Newton* spectra to avoid any cross-calibration problems, we see that the ratio HR between hard and soft fluxes (after correction for interstellar absorption) remained stable at all times, while the temperature and absorption also agree within errors. Clearly, the γ Cas characteristics did not disappear, nor did they change of relative strength, even though the flux changed and the disc evolved. Fig. 2 graphically displays this evolution of flux and hardness ratios over time. The top panel of the same figure compares the fluxes to the Hα line strength: It confirms the lack of correlation between X-ray parameters and the Hα line.

3.2 V767 Cen

At the start of the monitoring in 2019 March, the star displayed a rather strong emission, with the line amplitude nearly reaching four times the continuum level (Figs 3 and 4, EW ~ -8 Å). The line profile had a single peak, although with prominent shoulders (i.e. the line had a winebottle shape). The emission slowly decreased in April, and then went shortly back to its initial level in May, before resuming

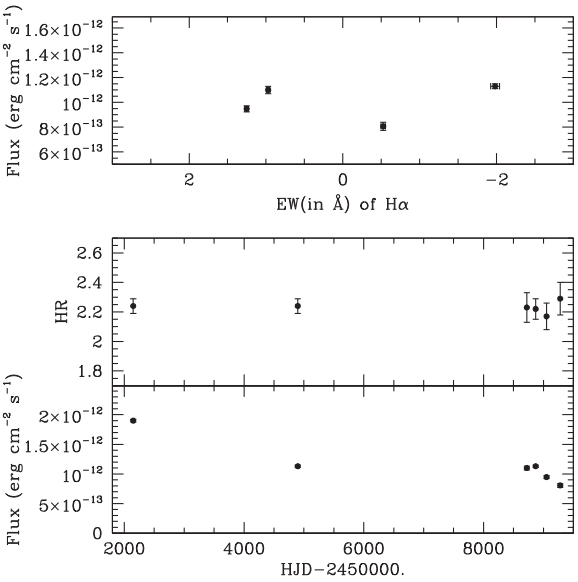

Figure 2. X-ray fluxes and hardness ratios of HD 119682 over time (bottom) and compared to EW (top).

its decrease. After this downward trend, the emission appeared to stabilize the next year. Only small variations were seen around an average EW of ∼–3 Å. At that time, the line profile reached an amplitude of only 1–1.5 times the continuum level. Furthermore, the shoulders seemed to have disappeared, while the broad stellar absorption started to appear in the high-velocity wings of the profile. The high-resolution ESO spectrum taken in 2020 September shows that the single peak seen in amateur data is actually made of two very close subpeaks. In 2020 December, the high-resolution ESO data revealed that the emission became narrower but of larger amplitude (EW = −4 Å, amplitude twice the continuum level, with clear hints of the photospheric absorption outside the emission range). The emission gradually decreased over the next months, down to EW = −2 Å, showing that the disc rebuilding was only temporary. In parallel, the separation between peaks in the double-peaked Hβ line profile changed from 18.5 km s^{-1} in early 2020 December to 52 km s^{-1} at the beginning of 2021 February. Using equation (2) of Zamanov et al. (2019), this translates into a size change for the emission region by a factor of ∼8 in just 2 months. Such a variation in peak separation is typical of Be discs as a larger disc reaches lower orbital velocities at its periphery than a small disc closer to the star (Hummel & Vrancken 1995; Zamanov et al. 2019).

The emission then stabilized in 2021 March–May, to finally resume its slow decrease in June. The absorption wings were clearly visible from mid-May to early July. While one would have expected the emission to slowly disappear, the absorption wings suddenly filled up. This suggests an input of fresh material close to the star, where velocities are large. In such a case, it is expected that the material will gradually spread out over the whole disc. Indeed, the core of the emission soon became broader and stronger, reaching one time the continuum level at the end of July (compared to an amplitude of one-half in mid-July). After this sudden event, the emission traced by the Hα line resumed its decrease.

Contrary to HD 119682, the Hα line was never largely dominated by absorption in our observations of V767 Cen, a clear emission being visible in all spectra, even at lowest EW. Both stars, however, display irregular decreases, often interrupted by short flaring episodes. Since the 2021 July flaring led to an EW increase never seen before in our monitoring, we decided to trigger X-ray observations to follow the reaction to the reinforcement of the disc, rather than to its disappearance as in HD 119682. *Swift* was the fastest to react, with the first exposure taken less than a week after the event, while the *XMM–Newton* data were taken a month later.

Comparing first the highest quality data, it is obvious that the 2007 and 2021 *XMM–Newton* spectra display very similar properties (absorption, temperatures, overall luminosity, and hardness ratio; see Table 3). Although the disc state in 2007 is not known, it would be quite a coincidence for it to be the exact same one as in 2021. In addition, each *XMM–Newton* light curve displays short-term flux variations, as found for HD 119682 and other γ Cas stars, but no hardness variations (see appendix, Fig. A2). Again, there seems to be no correlation between the overall count rate and the hardness in these light curves. Finally, while the disc emission was much lower in 2021 than at the beginning of the optical monitoring in 2019, the γ Cas character remained clear.

The *Swift* data allow us to examine the behaviour of the star in 2021 over a longer time-scale, albeit with lower quality data. V767 Cen appears slightly brighter in the second exposure and slightly fainter in the last ones, but the changes remain within 2σ: Again, the star seems to display a rather similar X-ray emission at all times. These results are shown in Fig. 5, which also graphically demonstrates the absence of correlation between X-ray flux and strength of the Hα line.

Finally, ASAS-SN provided photometry over a long time-scale[6] (see the top panel of Fig. 4). Despite their noise, those data clearly show that the broad-band photometry remains rather stable while the Hα line strongly changes.

4 DISCUSSION

4.1 Observed changes in γ Cas analogues

Among γ Cas analogues, only three stars had previously been followed through a transition of their disc. The Oe star HD 45314, the hottest γ Cas analogue known so far, was monitored extensively in the optical range (Rauw et al. 2018). X-ray observations were obtained as the star displayed very different disc states, as traced by the Hα line: strong emission (EW close to −23 Å), shell phase, and very small emission (EW of −7.9 Å). Changes in *V*-band photometry were also detected, indicating that even the inner parts of the disc were affected by the variation. Between the first and last observations, the X-ray flux was reduced by an order of magnitude and the hardness of the spectrum markedly decreased too (HR changed from 4.3 to 1.8; see Nazé & Motch 2018). The γ Cas character was thus disappearing, suggesting a direct link between the disc and the generation of X-rays (Rauw et al. 2018).

In contrast, the monitoring of π Aqr drew a different picture (Nazé et al. 2019). X-ray data were here also taken in two very different situations: as the disc had nearly completely disappeared (Hα EW of −1.7 Å) and as the emission associated with the disc was strong (EW of −23 Å, with a disc size five times larger). Here too, simultaneous variations in broad-band photometry were recorded. The first X-ray observation was a single *XMM–Newton* snapshot,

[6] V767 Cen was also observed by *TESS* during our monitoring campaign and these observations are reported in Nazé et al. (2020). Significant variations of about 0.2 mag were recorded by *TESS* over its few weeks' observing window and they are confirmed by the ASAS-SN data.

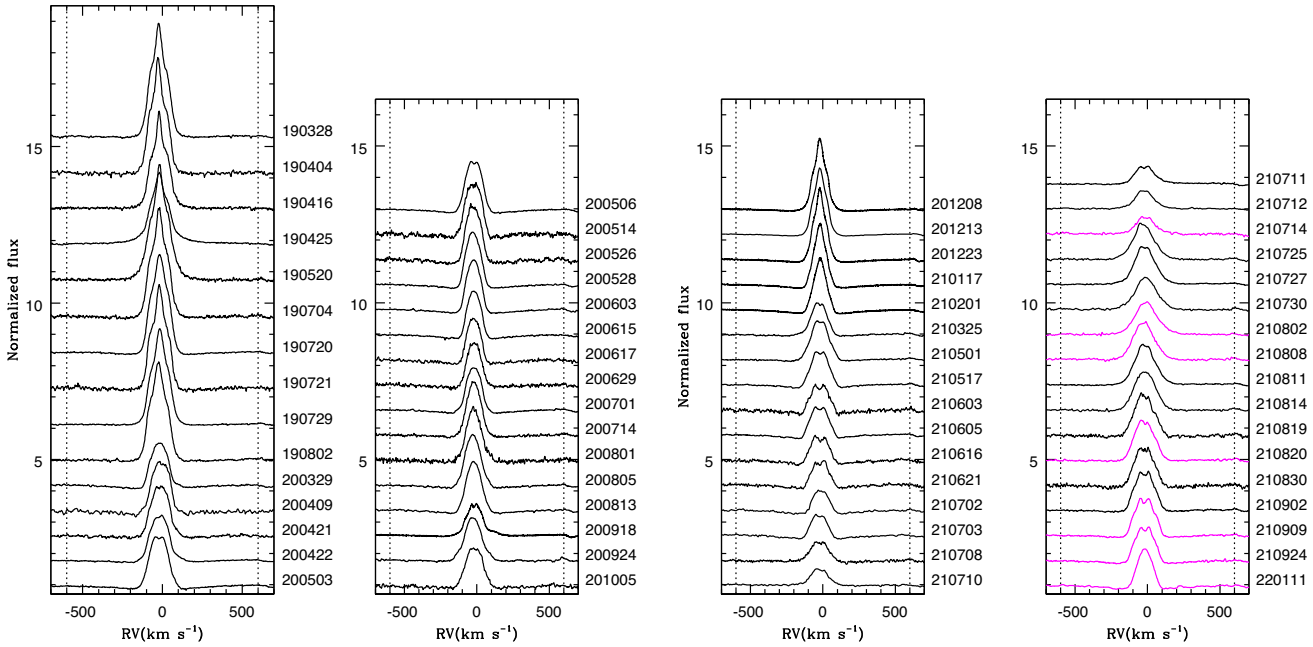

Figure 3. Same as the left-hand panel of Fig. 1 but for the profiles of V767 Cen. Note that low-resolution spectra here have $R < 5000$.

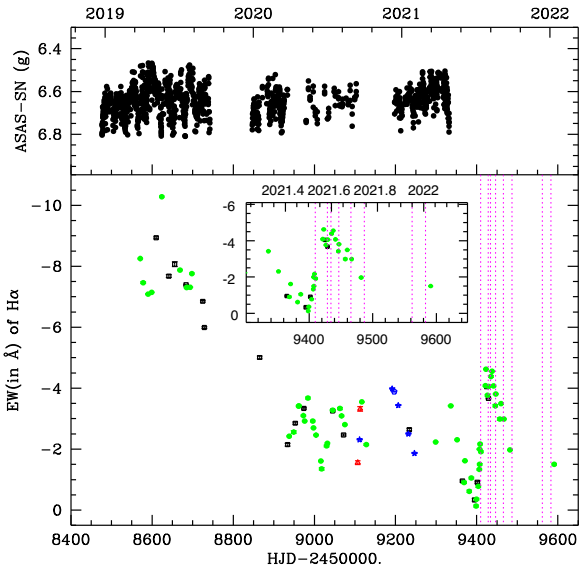

Figure 4. Top: *g*-magnitudes of V767 Cen recorded by ASAS-SN. Bottom: Same as the right-hand panel of Fig. 1 but for V767 Cen. Note that low-resolution spectra are here defined as $R < 5000$.

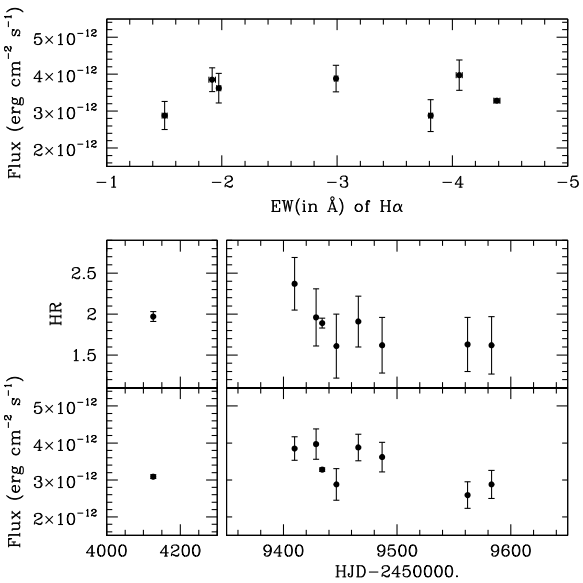

Figure 5. Same as Fig. 2 but for V767 Cen.

but the second observing campaign corresponds to a set of short exposures taken by *Swift* over 250 d (i.e. three orbital cycles). There was no obvious relation between the X-ray parameters derived from individual *Swift* exposures and the orbital phase or between them and the disc fluctuations of π Aqr as traced by Hα line strength (Nazé et al. 2019). To readdress this issue, we now combine the *Swift* exposures with the online tool[7] to get a single, higher quality spectrum. We fit it in the same way as done for the *XMM–Newton* spectrum in Nazé & Motch (2018); see Table 3 for results. While the short *Swift* exposures show individual fluxes varying by a factor of a few, as usual for the short-term intrinsic variations of γ Cas stars (Nazé et al. 2019), the flux of the combined *Swift* data set appears to be ∼50 per cent higher than that in the *XMM–Newton* data. This change is due to the increase of the hard X-ray flux, leading to a variation of the hardness ratio HR from 3.6 to 6.1. However, it is important to stress that the hard component was very clear and strong at all times. The γ Cas character thus never disappeared for π Aqr.

The third γ Cas star that has been simultaneously monitored at optical and X-ray wavelengths is γ Cas itself. Motch et al. (2015) reported a good correlation, without any time lag, between averages

[7] https://www.swift.ac.uk/user_objects/

over optical observing seasons of X-ray fluxes measured by *RXTE* and of disc brightnesses as traced by *V*-band magnitudes. Moreover, variations with time-scales near 70 d were found in both wavelength ranges. Recently, Rauw et al. (in preparation) reported on a set of *XMM–Newton* observations taken during an eruption event (with Hα EW transitioning from −45 Å to nearly −55 Å and then back to the initial value). They compared the high-energy emission then observed to that recorded in older *XMM–Newton* observations when the disc emission was significantly lower (Hα EW ranging from −27 to −35 Å). Both flux and hardness variations are observed in the X-ray range. Besides the usual short-term 'flaring' activity, the mean flux of each *XMM–Newton* observation varied by a factor of 2. The hardness ratio was similar in six out of the ten observations (HR ∼ 3) and three more observations displayed values rather close to that, despite the different strength of the Hα line at these nine dates. However, the X-ray spectrum clearly was hardest (HR ∼ 8) and faintest at the time of the maximum emission. This variation stems from the soft X-rays (the soft flux changed by a factor of 3–4), most probably because of a larger absorption. Such characteristics are reminiscent of the localized absorbing events reported by Hamaguchi et al. (2016) and Smith & Lopes de Oliveira (2019), of which this event would then be an extreme case. Indeed, the next exposure, taken only a month later when the Hα emission was still very strong, did not display those features. It can nevertheless not be totally excluded that the observed change is a direct high-energy reaction to the disc event. In any case, there was no obvious correlation between the Hα emission and the X-ray properties during this event or at previous epochs of *XMM–Newton* observations. Finally, it may be noted that no significant change in *V*-band photometry was detected during this recent emission event.

HD 119682 and V767 Cen add to this picture of contrasting behaviours. The X-ray flux of HD 119682 displayed long-term variations by a factor of 2, but the hardness of the emission remains stable (HR ∼ 2.2 in all *XMM–Newton* data). In particular, the γ Cas characteristics were still present when the optical spectrum showed no trace of emission (Hα EW of 1.3 Å). For V767 Cen, the disc never disappeared entirely: When it seemed on the edge of doing so (at an Hα EW of ∼−0.2 Å), the Hα emission suddenly increased. At X-ray wavelengths, however, the spectral properties show little change, both in flux and in hardness.

In summary, three disc disappearances (or near-disappearances) were monitored, for HD 45314 (O9pe), π Aqr (B1Ve), and HD 119682 (B0Ve). In all cases, a lower X-ray flux than observed before was measured at these times. However, the amplitude of the flux change wildly varied (an order of magnitude for HD 45314, about a factor of 2 for the other two). The hardness variations are even more different: HD 45314 had such a low hard X-ray emission that it formally lost its γ Cas character, the hardness of π Aqr decreased but the star still fulfilled the criteria to remain a γ Cas analogue, and HD 119682 kept the hardness measured before. This suggests the existence of a link, but a loose one, between the Hα emission of the disc and X-ray emissions.

In parallel, two disc 'flarings' were monitored, for γ Cas and V767 Cen. They were qualitatively very different, as the disc of γ Cas was already strong when it became stronger while that of V767 Cen was on the edge of disappearance when a disc rebuilding was detected. However, apart from a single *XMM–Newton* exposure of γ Cas, there was no large change of X-ray properties recorded in both stars. It is important to note that, for both stars, broad-band photometry showed no specific trace of flaring at the time of the recorded events [see above for V767 Cen, and see Rauw et al. (in preparation) for γ Cas].

4.2 The case of Be-XRBs

What do these monitoring results tell us on the generation of X-rays in γ Cas stars? To shed light on this issue, a comparison with the usual behaviour of Be stars in XRBs should be done. In such systems, the X-ray variability is often classified into two categories. Type I outbursts occur at specific orbital phases, when accretion is enhanced at periastron passages, while type II outbursts are rather linked to major disc changes, often after some reaction delay (e.g. Grundstrom et al. 2007; Camero-Arranz et al. 2012; Lutovinov, Tsygankov & Chernyakova 2012; Alfonso-Garzón et al. 2017). Most systems remain X-ray quiet when the Be disc is small or has disappeared (Negueruela et al. 2001), although a few systems have undergone type II outbursts even in such conditions (Monageng et al. 2017).

The X-ray observations of γ Cas analogues have not revealed any outburst up to now; hence, their closer analogues among XRBs may be the low-eccentricity systems such as X Per. From a long monitoring of this system, Zamanov et al. (2019) found a direct correlation, without time lag, between the X-ray flux and the EW of the Hα line. However, this occurred only when the emission was very strong, i.e. for a large disc. At lower emission levels, the situation was clearly different, with the *V*-band photometry varying first, then the EW(Hα), and at last the X-ray flux, after years of delay. This can be understood recalling that the accretion material comes from the outer parts of the disc: If the disc is small, it will take some time for such an inner variation to change the accreting conditions near the companion, while any variation at the periphery of a large disc, hence closer to the companion, will have a direct impact on the accretion flow.

4.3 Constraints on the γ Cas phenomenon

The γ Cas monitorings provide two important clues. First, the γ Cas character remained for π Aqr, HD 119682, and V767 Cen even when the Hα emission was very weak. Of course, the current Hα data do not enable us to conclude that the disc had entirely disappeared, even in the case of HD 119682. Indeed, though Hα is certainly a powerful diagnostics for the presence of a circumstellar disc, the line forms over a rather wide radial extent and is much less sensitive to the innermost and outermost parts of the disc. However, it is certain that the disc size was much reduced at these times. In fact, the size of the disc $R_{\rm d}$ can be evaluated from the peak separation $\Delta(V)$ in double-peaked profiles using $R_{\rm d} = R_* \times [2 \times v\sin(i)/\Delta(V)]^2$ (Huang 1972; Hummel & Vrancken 1995; Zamanov et al. 2019). The projected rotational velocities $v\sin(i)$ are 100 and 200 km s^{-1} for V767 Cen and HD 119682, respectively (Zorec et al. 2016). The peak separation was measured each time the profile appeared double peaked and this yielded disc sizes of a few R_* for HD 119682 and 10–30 R_* for V767 Cen. Comparable values were found for HD 45314 (Rauw et al. 2018) and π Aqr (Nazé et al. 2019). The disc sizes can also be evaluated from the EWs (see equation 3 in Zamanov et al. 2019), but the application of the formula can be debated for such small EW values (the largest |EW| measured here is around 10 Å). However, Reig et al. (2016) also found that the disc sizes must be small for such low EW. In our cases, the discs are thus smaller than those usually found in active states of Be-XRBs (see also fig. 5 of Zamanov et al. 2019). In any case, any compact companion would need to be very close for significant accretion (hence significant hard X-ray emission) to occur: If |EW| < 10 Å, then $P_{\rm orb} < 50$ d (see Coe & Kirk 2015). For a Be star mass of 12 $M_\odot$ and an Oe star mass of 20 $M_\odot$, a neutron star mass of 2 $M_\odot$, and a $P_{\rm orb} < 50$ d, the velocity amplitudes would be larger than 15–20 km s^{-1}, which is not

detected for HD 119682, V767 Cen, or HD 45314 (Rauw et al. 2018; Nazé et al. 2021). For π Aqr, the known orbital period is 84 d, with a disc much smaller than the orbital separation (Nazé et al. 2019, and references therein). The current data thus seem to disfavour scenarios involving accreting companions.

Secondly, the X-ray emission seems to react differently depending on the extent of the disc changes. Indeed, optical photometry and spectroscopy probe different zones of the disc: The stellar photometry is more sensitive to the densest and innermost parts of the disc, while the Hα line rather probes the disc over a larger region, up to its periphery. In γ Cas, HD 45314, and π Aqr, variations of the X-ray emission were spotted when both broad-band photometry and Hα line profile changed. In contrast, the recent 'events' in γ Cas and V767 Cen were detected through Hα measurements but both X-ray properties and optical broad-band photometry remained unaffected. All this may be a hint that the hard X-ray emission that characterizes the γ Cas phenomenon is born in the inner discs of the Be stars, rather than at their periphery.

The observed optical and X-ray behaviours of γ Cas analogues therefore reveal that the γ Cas character may remain even if the disc size is much reduced and that changes in X-rays are usually seen only if broad-band photometric variations occurred. This is difficult to reconcile with a crucial role of distant companions, and seems to bring support to the magnetic star–disc interactions where X-rays are generated closer to the Be star (Robinson et al. 2002). The differences observed between γ Cas analogues could then result from a range of reasons such as varying inclinations, stellar rotation, and stellar temperatures. For example, the hotter Oe star HD 45314 should have a stronger wind and a faster disc disappearance (Kee, Owocki & Sundqvist 2016). In contrast, the disc of the cooler Be stars would take more time to disperse; hence, rebuilding events would have time to occur and a full disc disappearance may be more difficult to get. With the inner parts of the disc still in place, the γ Cas character would then still be observable. Nevertheless, no full modelling of the star–disc interaction is available yet; hence, it is difficult to exactly quantify its adequacy. Future modelling should explore the specific impact of geometry and stellar properties.

5 SUMMARY AND CONCLUSION

The Hα line in Be stars is considered as one of the main probes of their discs. We have monitored this line for two γ Cas analogues, namely HD 119682 and V767 Cen, for several years. Both stars displayed decreasing line strengths, although interrupted by several short rebuilding events. The discovery of this behaviour triggered X-ray observations, to assess the impact of the disc changes on the peculiar high-energy emission of those stars.

For HD 119682, the Hα line was fully in absorption in 2020 mid-July. In parallel, the X-ray flux slightly decreased between 2019 August and 2021 March, with no change in hardness. The flux level was comparable to that recorded a decade before in a previous X-ray exposure. The γ Cas character remained clear at all epochs.

V767 Cen was monitored during a disc rebuilding event and no significant change in X-ray flux or hardness was detected. In parallel, ASAS-SN photometry in the visible range also appeared to remain stable.

The limited reaction to large Hα variations and the presence of the γ Cas character even with a weak Hα line, coupled to a stable photometry, seem to disfavour scenarios involving an X-ray source located far out in the disc, close to a companion, and rather hint at an X-ray generation closer to the Be star.

These results brought important clues regarding the γ Cas phenomenon, but of course much remains to be done. In particular, the optical and X-ray monitorings should continue, to exclude large time delays and/or to analyse the X-ray behaviour during long (and complete) disc disappearances. Also, while the disc clearly plays some role in the appearance of the γ Cas phenomenon (since all γ Cas are Be stars), it remains to be clarified why most Be stars are not γ Cas in character.

ACKNOWLEDGEMENTS

We thank Dr N. Schartel for granting us a DDT observation of V767 Cen and the *Swift* team for their help. We also thank Myron Smith for his comments and useful discussions. YN and GR acknowledge support from the Fonds National de la Recherche Scientifique (Belgium), the European Space Agency (ESA), and the Belgian Federal Science Policy Office (⟨0:funding-source 3:href="http://dx.doi.org/10.13039/501100002749"⟩BELSPO⟨/0:funding-source⟩) in the framework of the PRODEX Programme (contracts linked to *XMM–Newton* and *Gaia*). ADS and CDS were used for preparing this document.

This study is based on *XMM–Newton*, *Swift*, and ESO data.

DATA AVAILABILITY

The ESO, *Swift*, *Chandra*, and *XMM–Newton* data used in this article are available in their respective public archives, while the Australian optical amateur spectra are available in the public BeSS data base (http://basebe.obspm.fr/basebe/). The Brazilian amateur data are available upon reasonable request.

REFERENCES

Alfonso-Garzón J. et al., 2017, A&A, 607, A52
Asplund M., Grevesse N., Sauval A. J., Scott P., 2009, ARA&A, 47, 481
Camero-Arranz A. et al., 2012, ApJ, 754, 20
Coe M. J., Kirk J., 2015, MNRAS, 452, 969
Feldmeier A., Puls J., Pauldrach A. W. A., 1997, A&A, 322, 878
Grundstrom E. D. et al., 2007, ApJ, 660, 1398
Hamaguchi K., Oskinova L., Russell C. M. P., Petre R., Enoto T., Morihana K., Ishida M., 2016, ApJ, 832, 140
Huang S.-S., 1972, ApJ, 171, 549
Hummel W., Vrancken M., 1995, A&A, 302, 751
Kee N. D., Owocki S., Sundqvist J. O., 2016, MNRAS, 458, 2323
Langer N., Baade D., Bodensteiner J., Greiner J., Rivinius T., Martayan C., Borre C. C., 2020, A&A, 633, A40
Lutovinov A., Tsygankov S., Chernyakova M., 2012, MNRAS, 423, 1978
Monageng I. M., McBride V. A., Coe M. J., Steele I. A., Reig P., 2017, MNRAS, 464, 572
Motch C., Lopes de Oliveira R., Smith M. A., 2015, ApJ, 806, 177
Murakami T., Koyama K., Inoue H., Agrawal P. C., 1986, ApJ, 310, L31
Nazé Y., Motch C., 2018, A&A, 619, A148
Nazé Y., Rauw G., Czesla S., Smith M. A., Robrade J., 2021, MNRAS, 510, 2286
Nazé Y., Rauw G., Pigulski A., 2020, MNRAS, 498, 3171
Nazé Y., Rauw G., Smith M., 2019, A&A, 632, A23
Negueruela I., Okazaki A. T., Fabregat J., Coe M. J., Munari U., Tomov T., 2001, A&A, 369, 117
Neiner C., de Batz B., Cochard F., Floquet M., Mekkas A., Desnoux V., 2011, AJ, 142, 149
Postnov K., Oskinova L., Torrejón J. M., 2017, MNRAS, 465, L119
Rakowski C. E., Schulz N. S., Wolk S. J., Testa P., 2006, ApJ, 649, L111
Rauw G. et al., 2018, A&A, 615, A44
Rauw G., Nazé Y., 2016, Adv. Space Res., 58, 761

Reig P., Nersesian A., Zezas A., Gkouvelis L., Coe M. J., 2016, A&A, 590, A122
Robinson R. D., Smith M. A., Henry G. W., 2002, ApJ, 575, 435
Safi-Harb S., Ribó M., Butt Y., Matheson H., Negueruela I., Lu F., Jia S., Chen Y., 2007, ApJ, 659, 407
Smith M. A., Lopes de Oliveira R., 2019, MNRAS, 488, 5048
Smith M. A., Lopes de Oliveira R., Motch C., 2012, ApJ, 755, 64
Smith M. A., Lopes de Oliveira R., Motch C., 2016, Adv. Space Res., 58, 782
ud-Doula A., Nazé Y., 2016, Adv. Space Res., 58, 680
Zamanov R., Stoyanov K. A., Wolter U., Marchev D., Petrov N. I., 2019, A&A, 622, A173
Zorec J. et al., 2016, A&A, 595, A132

APPENDIX: X-RAY LIGHT CURVES

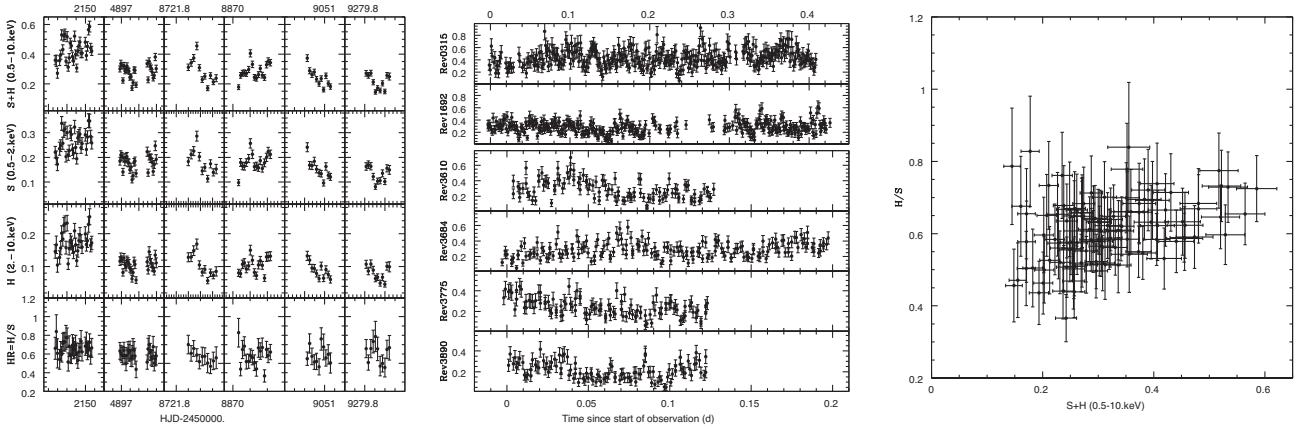

Figure A1. Left-hand panels: *XMM–Newton* light curves of HD 119682 in several energy bands and with a time bin of 1000 s. Middle panels: *XMM–Newton* light curves of HD 119682 in the total energy band and with a time bin of 100 s. Right-hand panel: Hardness ratio as a function of the total count rate in all *XMM–Newton* light curves of HD 119682 with a time bin of 1000 s.

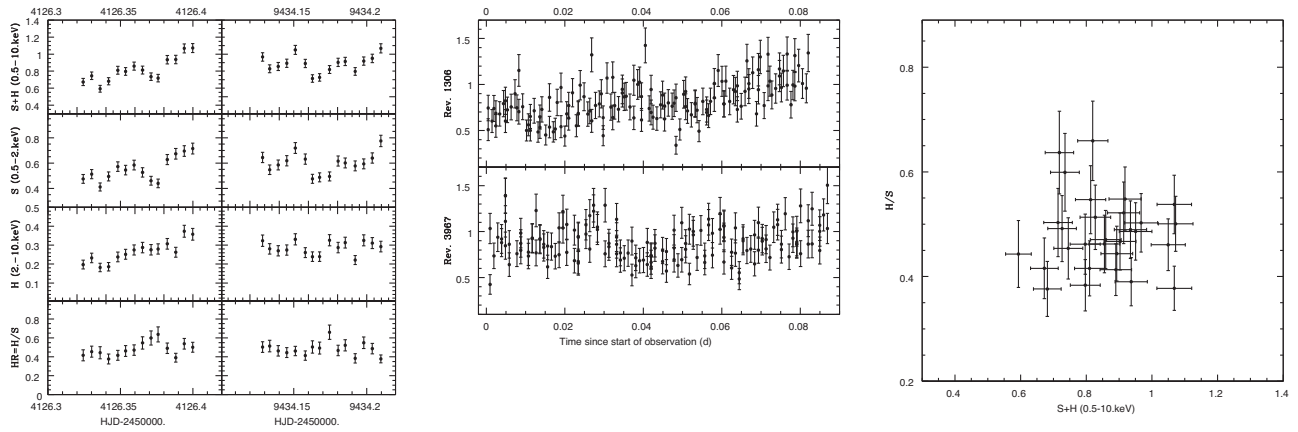

Figure A2. Left-hand panels: *XMM–Newton* light curves of V767 Cen in several energy bands and with a time bin of 500 s. Middle panels: *XMM–Newton* light curves of V767 Cen in the total energy band and with a time bin of 50 s. Right-hand panel: Hardness ratio as a function of the total count rate in all *XMM–Newton* light curves of V767 Cen with a time bin of 500 s.

This paper has been typeset from a TEX/LATEX file prepared by the author.